

Deriving Fast AC OPF Solutions via Proximal Policy Optimization for Secure and Economic Grid Operation

Yuhao Zhou, *Student Member, IEEE*, Bei Zhang, *Member, IEEE*, Chunlei Xu, Tu Lan, Ruisheng Diao, *Senior Member, IEEE*, Di Shi, *Senior Member, IEEE*, Zhiwei Wang, *Senior Member, IEEE*, and Wei-Jen Lee, *Fellow, IEEE*

Abstract—Solving AC optimal power flow (OPF) with operational security constraints remains an important but challenging optimization problem for secure and economic operations of the power grid. With the ever-increasing penetration of renewable energy, fast and large fluctuations in power and voltage profiles are observed on a daily basis; thus, fast and accurate control actions derived in real-time are needed to ensure system security and economics. This paper presents a novel method to derive fast OPF solutions using state-of-the-art deep reinforcement learning (DRL) techniques, which can greatly assist grid operators in making rapid and effective decisions. Imitation learning (IL) is adopted to generate initial weights for the neural network (NN); and more importantly, proximal policy optimization (PPO) algorithm is utilized to train and test stable and robust AI agents. The training and testing procedures are conducted on both the IEEE 14-bus and the Illinois 200-bus systems. The results demonstrate the effectiveness of the proposed methodology and illustrate its great potential for assisting grid operators in real-time operation.

Index Terms—AC optimal power flow, deep reinforcement learning, imitation learning, and proximal policy optimization.

I. INTRODUCTION

WITH a high penetration of fluctuating energy resources being integrated into modern power grids such as renewable energy, today’s power grid is facing bigger challenges in real-time operation. Fast and accurate control actions are needed to ensure system security and economics. Therefore, there is a compelling need for fast AC OPF solutions for real time applications [1].

A number of dedicated approaches were proposed to solve the non-convex AC OPF problem in recent decades. The primal-dual interior-point method was applied in [2]; the convex relaxation method to tackle the AC OPF problem for radial networks via applying second-order cone programming (SOCP) was firstly proposed in [3]. In [4]-[7], semidefinite programming (SDP) for meshed networks was proposed and the exactness of achieving the global optimum point was discussed. However, all aforementioned methods require massive time to converge, especially for large-scale systems,

which prevents them from being deployed in real-time applications. Sub-optimal solvers are used among industry to compromise the computational time requirement. Nearly all vendors’ tools adopt assumption and simplification to reach feasible and suboptimal solutions for real-world implementation, e.g., DC-based power flow equations with relaxed security constraints. To address this issue, a single-iteration quasi-Newton method was proposed to expedite the solution process in [1] with the prerequisite for an accurate estimation of the second-order information. Linearized AC power flow equations were reported to achieve real-time OPF in distribution systems in [8]. Recently, several supervised-learning-based methods are reported to approximate OPF solutions. In [9], a graph neural network is applied to approximate the solutions of power flow solvers. Meanwhile, deep neural networks (DNN) are utilized to solve the DC OPF [10]-[11] and AC OPF problem [12]-[13]. These methods mainly use supervised learning techniques to train neural networks using massive simulations obtained beforehand for approximating optimal solutions; thus it may limit their performance when the feasible regions are small for the AC OPF problem with full security constraints.

The recent success of DRL algorithms in many control problems such as games, robotics, autonomous driving, and finance provides a promising alternative for power system decision making [14]. A well-trained DRL agent does not rely on full system models when making control decisions, which can respond instantaneously to various conditions that enable real-time applications. Recently, several DRL-based applications are reported in the smart grid area. In [15], the multi-agent Q-learning method was applied to optimal reactive power dispatch. In [16], multi-agent $Q(\lambda)$ learning was adopted to perform OPF tasks under discretized action spaces with grid partitioned. In [17], the deep Q network (DQN) was utilized to perform optimal control for smart buildings. In [18]-[19], a novel platform “Grid Mind” was proposed and the DQN and the deep deterministic policy gradient (DDPG) algorithms were implemented to perform autonomous voltage control. In [20], the DDPG algorithm was applied for the load frequency control.

Inspired by the efforts above, this paper proposed a novel

Y. Zhou was a summer research intern with GEIRI North America, San Jose, CA 95134 USA. B. Zhang, T. Lan, R. Diao, D. Shi, and Z. Wang are with GEIRI North America, San Jose, CA 95134 USA. (e-mail: {bei.zhang, tu.lan, ruisheng.diao, di.shi, zhiwei.wang}@geirina.net).

C. Xu is with State Grid Jiangsu Electric Power Company, Nanjing, China. (email: chunleixu@js.sgcc.com.cn).

Y. Zhou and W. Lee are with the Electrical Engineering Department, University of Texas at Arlington, Arlington TX 76019 USA. (e-mail: yuhao.zhou@mavs.uta.edu; wlee@uta.edu).

DRL-based method to derive a near optimal solutions for the AC OPF problem that has the potential in real time applications. With the implementation of the DRL to train the DNN, it could significantly improve the solving success rate, especially when the feasible region is small. Different from most of the aforementioned efforts, continuous control action space is considered in this effort, corresponding to the actual needs of power grid control, which alleviates the compromise in performance as well as the “curse of dimension” caused by discretization of control action. Therefore, the grid does not have to be partitioned to introduce further approximation or inaccuracy like [16]. Besides, the state-of-the-art PPO algorithm [21] is employed to train the agent to solve the AC OPF problem. Different from DDPG, the PPO algorithm tries to ensure safe updates within certain trust regions, which greatly improves its robustness, performance, and extensibility to systems of larger sizes. To further guarantee the success in training as well as to expedite the entire training process, the IL technique is utilized to obtain an initial policy weight for better training in the DRL process. Numerical experiments conducted on two power grid models demonstrate that the results of the proposed approach are comparable with one of the most popular AC OPF solver in PYPOWER [22] (python version of MATPOWER[23]) but with significant improvement on the computational time, which manifests a great promise of employing AI techniques in the future power system control and operations.

The remainder of the paper is organized as follows: Section II provides the principles of DRL, IL, and PPO algorithms. In section III, the detailed procedures of the proposed methodology are illustrated. In Section IV, numerical experiments are conducted using both the IEEE 14-bus and the Illinois 200-bus systems to demonstrate the performance of the DRL and the effectiveness of the proposed method. Finally, Section V concludes the work and presents future work.

II. PRINCIPLES OF DRL, IL AND PPO ALGORITHM

A. DRL Basis

The goal of reinforcement learning (RL) is to maximize a long-term expected reward by continuously interacting with the environment as depicted in Fig. 1 [14], where s_t is the observed state by the agent at time step t , a_t is the agent’s action according to the current policy π at time step t , r_t is the immediate reward from the environment at time step t . After executing action a_t , the environment transits to the next state s_{t+1} . By unceasingly interacting with the environment, the agent’s policy *rollouts* and forms a *trajectory*. During such process, the set of states \mathcal{S} , the set of actions \mathcal{A} , the transition probability $\mathcal{T}(s_{t+1}|s_t, a_t)$, which maps the distribution of the next state with the current (state, action) pair, the set of reward $\mathcal{R}(s, a, r)$, and a discount factor $\gamma \in [0, 1]$ on the future reward together form a Markov decision process denoted as a tuple $\langle \mathcal{S}, \mathcal{A}, \mathcal{T}, \mathcal{R}, \gamma \rangle$.

Every trajectory of a policy returns an accumulated reward shown in Eq. (1) [24]. And the agent aims at learning an optimal policy π^* that maximizes the expected return.

$$R_t = \sum_{k=0}^{\infty} \gamma^k r_{t+k+1} \quad (1)$$

Two other important concepts of RL are state-value and action-value functions as defined in Eq. (2) and Eq. (3), respectively [24].

$$V^\pi(s) = E(R_t | s_t = s; \pi) \quad (2)$$

$$Q^\pi(s, a) = E(R_t | s_t = s, a_t = a; \pi) \quad (3)$$

State-value function $V^\pi(s)$ represents how good a state is by calculating the expected reward starting from such state following a certain policy; whereas action-value function $Q^\pi(s, a)$ assesses how good an action is at a certain state by evaluating the expected reward starting from the state s with the action a following a policy π .

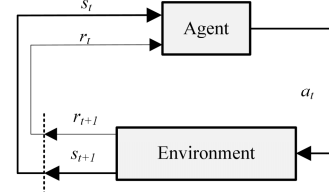


Fig. 1. A brief description of the RL training process.

Combining deep learning (DL) algorithms [25] with RL defines the fields of DRL. In the DRL, the deterministic or the stochastic policy $\pi_\theta(a_t|s_t)$ is usually approximated by a NN with parameters θ , which represents the weights and biases in the NN. And the agent learns to update θ such that the optimal policy is achieved.

B. IL Technique

Imitation learning, or learning by demonstration, focuses on imitating experts’ demonstrations [26]. The goal of IL is to learn a policy that maps the states to actions, which is similar to the DRL. Nonetheless, the training technique is a bit different, with Dataset Aggregation algorithm (DAgger) usually adopted. Starting from running a standard supervised imitation learning, by following the previous trained policy to collect new trajectories but recording the expert’s behavior, new tuple (state, expert’s action) pairs are formulated and aggregated as an updated training dataset to further train the policy until it converges [26]. Due to the close connection between the DRL and the IL, the training result of the IL could be adopted as the initialization of the policy NN for the DRL, which would: 1) alleviate the computational feasibility problems in DRL (the problem with sparse reward may confuse the agent and result in failure in finding the policy); 2) solve the sample-inefficiency caused by numerous trial and error without experts’ demonstration; and 3) make the training safer by avoiding catastrophic consequence due to expert’s knowledge [27].

C. PPO with Clipped Surrogate Loss

Policy gradient (PG) algorithm [24] optimizes the policies directly by adopting the stochastic gradient ascent algorithm. Nevertheless, the conventional PG algorithm does not have a good convergence especially with high dimensional and/or continuous action spaces [21]. Originated from the PG algorithm, the PPO algorithm is proposed to ensure a better convergence, which is achieved by: 1) the *actor-critic* structure: an actor NN to learn the stochastic optimal policy and a critic NN to estimate the value function; and 2) two other

enhancements illustrated as follows.

Firstly, the generalized advantage estimation (GAE) function $A_t^{GAE(\gamma, \lambda)}$ is utilized to replace Eq. (3) during the update in order to reduce the variance of the estimation, which is shown in Eq. (4) [28], where $V^\pi(s_t)$ is the state value shown in Eq. (2) starting from time step t , which comes from the critic NN; λ controls the averaging degree of n-step advantage values [28].

$$\begin{cases} A_t^{GAE(\gamma, \lambda)} = (1 - \lambda)(\hat{A}_t^{(1)} + \lambda \hat{A}_t^{(2)} + \lambda^2 \hat{A}_t^{(3)} + \dots) \\ \hat{A}_t^{(k)} = \sum_{i=0}^{k-1} \gamma^i \delta_{t+i}^V = -V^\pi(s_t) + r_t + \gamma r_{t+1} + \dots + \gamma^{k-1} r_{t+k-1} + \gamma^k V^\pi(s_{t+k}) \end{cases} \quad (4)$$

On the other hand, the PPO updates the parameters within an appropriate trust-region [29], and this helps avoid falling off the “cliff” from the hyper-surfaces of the complex reward functions which may be hard to escape from. Such a safe update is achieved by modifying the objective function L shown in Eq. (5), where θ indicates parameters of the actor NN $\pi_\theta(a_t|s_t)$; ε determines the range of the trust-region for the update; advantage value A_t is calculated from Eq. (4) $A_t^{GAE(\gamma, \lambda)}$. The minimization operator makes sure that the new policy does not benefit from going too far away from the old policy and thus regulating the update of the parameter.

$$\begin{aligned} L(\theta) &= \hat{E}_t[\min(r_t(\theta) A_t^{\pi_{old}}, \text{clip}(r_t(\theta), 1 - \varepsilon, 1 + \varepsilon) A_t^{\pi_{old}})] \\ \text{where } r_t(\theta) &= \frac{\pi_\theta(a_t | s_t)}{\pi_{\theta_{old}}(a_t | s_t)} \end{aligned} \quad (5)$$

The policy π_θ is stochastic in PPO, which is parameterized as a conditional Gaussian policy $\pi_\theta \sim N(\mu_\theta(s), \Sigma_\theta)$. The mean vector $\mu_\theta(s)$ is the output of the actor NN, and the covariance Σ_θ is a diagonal matrix initially assigned manually but would be updated during the backpropagation. Besides, θ_{old} is the policy parameters before the actor NN’s update.

As for the critic NN, its objective function is shown as follows.

$$\min_{\varphi} \sum_{(s_t, R_t) \in \mathcal{D}_{batch}} \frac{1}{N_{batch}} \|R_t - V_\varphi^\pi(s_t)\|_2^2 \quad (6)$$

where R_t is the discounted accumulated reward from Eq. (1), \mathcal{D}_{batch} is the trajectories with batch size N_{batch} , and φ represents parameters of the critic NN.

III. DRL BASED AC OPF WITH IL

The goal of the DRL agent is to minimize total generation cost without violating operational constraints or shedding the load, by controlling the voltage set-points and power outputs of generators under various loading conditions. The agent can be trained offline through historical data or/and massive simulations and then applied on-line in the real grid. During the on-line application, a well-trained agent is capable of providing control actions momentarily regardless of the system size. This section mainly focuses on the efficient off-line training process of such agent, which includes the design of several important components during DRL training: off-line grid environment, state and action spaces, neural network structures, IL implementation, and the detailed training process.

A. Off-line Grid Environment

In this paper, the off-line environment is developed by mimicking the OpenAI Gym environments (benchmark

systems for the DRL studies [30]), which consists of an AC power flow (PF) solver and several important functions, shown below:

Initialization: “*reset()*” function initializes a case by running the PF and outputs the initial state s_t ;

Interaction: “*step()*” function applies the agent’s action, runs the PF, and then provides the agent with the resulting state, “*done*” signal and the corresponding reward;

Reward calculation: the detailed design for the reward function is presented in Eq. (7), where R_{pg_v} , R_{v_v} , and R_{br_v} correspond to the negative reward if any inequality violation is detected on: (1) the active power limits of generators; (2) the voltage magnitude limits of buses; and (3) the branch thermal flow limits (in both directions) of transmission lines. Coefficients k and b are applied to map the positive reward (when no violation) under various situations into a similar range, for example, $[0, 500]$, to facilitate the training process; and the coefficient z is considered as a correction item to compensate for the previous mapping errors such that the positive reward is guaranteed when there are no violations of operational constraints. $C_{generators}$ represents the generator costs.

$$\text{reward} = \begin{cases} -5000, & \text{if PF solver is diverged} \\ R_{pg_v} + R_{v_v} + R_{br_v}, & \text{if there are constraints violations} \\ k \times C_{generators} + b + z, & \text{if system is normal} \end{cases} \quad (7)$$

Fig. 2 illustrates the interaction between the DRL agent and the off-line grid environment during one episode, which starts from the initialization on the case through “*reset()*” until the “*end*” in the figure with “*done*” set to “*True*” by “*step()*”. Different from the OpenAI Gym environments, the “*done*” signal, which usually indicates whether the desired state is reached, is hard to determine in this case, since it is difficult to determine whether the optimal cost has been reached. Therefore, in our environment, the “*done*” signal becomes “*True*” when (1) the power flow result diverges; or (2) the maximum number of steps has been reached.

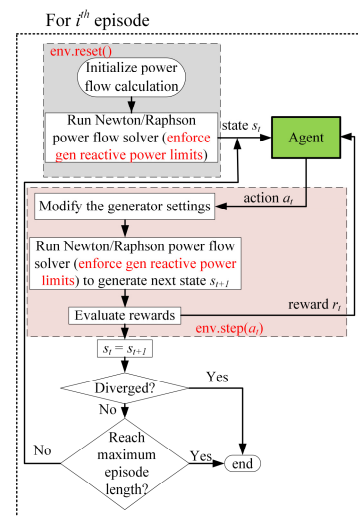


Fig. 2. The flowchart of the grid environment interacting with an agent.

B. State and Action Spaces

The state, which is the input for the DRL agent, includes the active and reactive power of the load, P_{di} and Q_{di} at each bus i ,

and the initial active power setting P_{gj} and voltage setting V_{gj} for every generator j , as denoted in Eq. (8), where n is the number of loads, and t is the number of generators in a grid. The *MinMax* scaling preprocessing [31] needs to be conducted on this vector before passing it to the agent to handle different scaling of various parameters.

$$state = [P_{d1}, \dots, P_{dn}, Q_{d1}, \dots, Q_{dn}, P_{g1}, \dots, P_{gm}, V_{g1}, \dots, V_{gt}] \quad (8)$$

As for the action space, it consists of generator settings' adjustments which is presented in Eq. (9). Such selection on the action can further correlate the states and actions.

$$action = [\Delta P_{g1}, \dots, \Delta P_{gm}, \Delta V_{g1}, \dots, \Delta V_{gt}] \quad (9)$$

C. Neural Network Structure in PPO Training

The actor and critic structures in PPO are shown in Fig. 3 and Fig. 4, respectively, the inputs for which are denoted in Eq.(8). The rectified linear unit (*ReLU*) activation function in the hidden layers can effectively prevent the vanishing gradient, and the *sigmoid* activation in the actor output layer makes sure the output can have bounded negative or positive values. The one neuron in the critic output layer has no activation, which outputs the value function of a given state.

One special design on the actor NN, as shown in Fig. 3, greatly improves the convergence of the network: only active and reactive loads are fed as the input of the NN in the actor, and the difference between the output of the NN and the voltage settings together with the active power outputs are then finally set as the actions, as denoted in Eq. (9), which is illustrated in Fig. 3.

There are three main considerations behind such design to achieve desired performance: 1) the OPF results are mainly determined by load variations and operational constraints; 2) to achieve better performance of NN, it is helpful to simplify its mapping logic: mapping the optimal settings alone would be much easier than directly mapping the actions because of the fact that the action can be the difference between the optimal and the initial generator settings; 3) such design does not require very accurate initial generator settings, and even if the initial power flow diverges, the structure would still be able to provide the optimal actions.

D. IL Implementation

IL can help initialize the weights for the actor NN and therefore speed up the DRL agent training process. For control problems with large state and action spaces, learning from scratch may even fail during the training process. In this work, we adopt the DL technique to conduct the IL for the actor NN, since: 1) we target at solving the problem in just one step; 2) the mapping between the load and the optimal generator settings does not involve the trajectory of multi-step interactions with the environment within one episode. The IL training method adopted in this paper is very similar to [12].

The "expert" actions for optimal generator settings could be obtained by running AC OPF solver offline for training dataset \mathcal{D}_{train} with a size of N_{IL} . Afterward, these (state, "expert" action) pairs are utilized in DL to initialize the actor NN, where the inputs are the states and the "labels" are the "expert" actions. By adopting Eq. (10) as the loss function via the first-order

optimizer such as Stochastic Gradient Descent, the initial mean value $\mu_{\theta}(s)$ of the stochastic policy π_{θ} in PPO agent could be trained to clone the optimal generator settings from OPF solver results.

$$\min_{\theta} \sum_{(s_t, a_t) \in \mathcal{D}_{train}} \frac{1}{N_{IL}} \|\hat{a}_t - \mu_{\theta}(a_t|s_t)\|_2^2 \quad (10)$$

On the other hand, the IL training result could serve as a validation for the structure of the actor NN. Fig. 5 exemplifies a comparison of the loss during the training process between two different designs on the actor NNs using one scenario of the IEEE 14-bus system. These two NNs have the same structure of hidden layers but different input layers: the structure of the NN at the top left in Fig. 5 is the same as the one illustrated in Fig. 3; the NN at the bottom left in Fig. 5 directly maps all inputs including load and generators' initial settings to the action space as shown in Eq. (9).

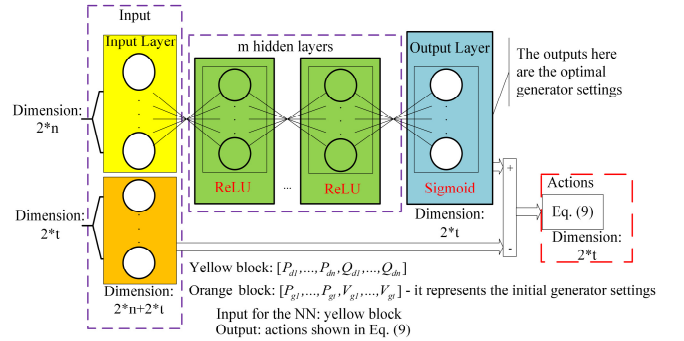


Fig. 3. "Actor" Neural Network structure in PPO training.

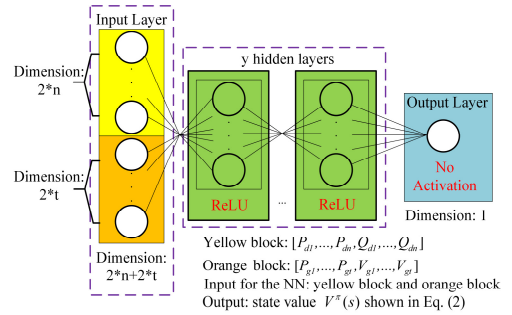


Fig. 4. "Critic" Neural Network structure in PPO training.

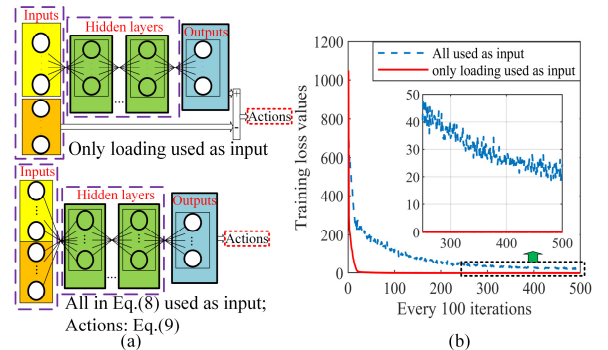


Fig. 5. IL comparisons based on 2 different NN structures. (a) NN's structure. (b) Training loss.

From Fig. 5, it's clearly seen that the training loss of the NN with the proposed structure in Fig. 3 is much smaller than that

of the NN that includes all information in Eq. (8) as the input (actually the loss shows the training does not converge under such design), which verifies the significant advantages of our design for the actor NN.

However, IL alone here is not enough, which will be further illustrated in Section IV, since it is very difficult to generate enough good samples that are representative of all different operating conditions [24] through DL alone. The DRL process thus needs to be adopted to further train the control policy for better control performance.

E. Detailed PPO Training Algorithm in Solving the AC OPF Problem

The training process of the DRL agent can generate data that cover representative situations during the agent’s interaction with the environment. By combing IL and DRL, their corresponding advantages can be maximized. The detailed PPO training algorithm is shown in Algorithm I.

Algorithm I PPO training for solving the AC OPF problem

- 1: **initialize:** the number of training data E_{p_max} , episode length T , discounting factor γ , λ in Eq. (4), KL_tar , batch size N_{batch} in Eq. (6), policy log covariance Σ_{π_0} , training epoch number epo , actor NN $policy$, critic NN $valuefn$, updating NN number N_{NN}
 - 2: parse in the training dataset \mathcal{D}_{train} containing the information of load and generator settings
 - 3: **for** each $epoch$ in range(epo):
 - 4: shuffle the training data and set $index = 0$
 - 5: **while** $index < E_{p_max}$:
 - 6: get a new batch of data with batch size N_{batch}
 - 7: **for** each episode e in range(N_{batch}):
 - 8: collect the trajectories’ information for every step including (s_t, a_t, r_t, s_{t+1}) from Fig. 2
 - 9: **end for**
 - 10: **for** $_$ in range(N_{NN}):
 - 11: optimize Eq. (5) wrt θ via Adam optimizer
 - 12: **break if** $KL\text{-divergence} > KL_tar$:
 - 13: **end for**
 - 14: **for** $_$ in range(N_{NN}):
 - 15: optimize Eq. (6) wrt ϕ via Adam optimizer [33]
 - 16: **end for**
 - 17: $index = index + N_{batch}$;
 - 18: **end while**
 - 19: **end for**
 - 20: **return:** $policy$
-

In Algorithm I, one $epoch$ means that all the training data have been trained once in the DRL. In addition, $KL\text{-divergence}$ measures the difference between two distributions, as defined in Eq. (11), where P and Q are two probability distributions with individual probability density function $p(x)$ and $q(x)$, respectively [32].

$$D_{KL}(P \parallel Q) = \int_{-\infty}^{\infty} p(x)(\log(p(x)) - \log(q(x)))dx \quad (11)$$

Moreover, the hyper-parameter KL_tar controls the dynamic training updates for the actor NN, which additionally overlooks

the balance between explorations and exploitations in PPO.

The brief training and testing approaches in this paper is summarized in Fig. 6. After the imitation learning to initialize the agent to further conduct the PPO training, the trained agent can be evaluated to solve AC OPF which will be discussed in Section IV.

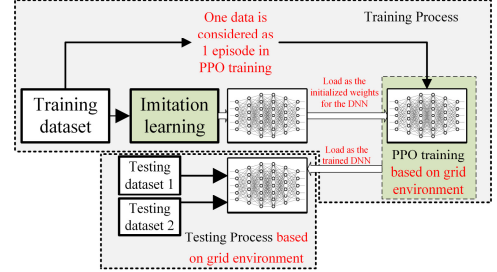


Fig. 6. Architecture and information flow of the proposed method to solve the AC OPF problem.

IV. CASE STUDY

The proposed approach to solving the AC OPF problem is tested on both the IEEE 14-bus [34] (with 14 buses, 5 generators, and 20 lines) and the Illinois 200-bus [35] (with 200 buses, 38 generators, and 245 lines) systems. The simulation platform is developed using Python 3.7, and the offline grid environment is established on the PF solver in PYPOWER, which provides Newton-Raphson PF solver and interior-point AC OPF solver (PIPS). The main objective is to minimize total generation cost without violating security constraints including voltage secure zones and thermal limits of transmission lines, for the base operating scenarios. No N-1 or N-2 security constraints are considered yet in the case studies.

Data generation: each load is randomly perturbed between [0.6 p.u., 1.4 p.u.] with uniform distribution; each generator’s setting is also randomly perturbed between $[P_{gmin}, P_{gmax}]$ for active power control and $[V_{gmin}, V_{gmax}]$ for reactive power control.

Label creation: the embedded PIPS is adopted to generate the optimal action labels for IL, and to indicate whether the OPF problem is feasible or not.

Data arrangement: all the data with feasible OPF solution are collected and divided into 3 datasets for different purposes shown in Fig. 6: **training dataset** – used for IL and PPO training, and contains the cases that can be solved by the PF solver; **testing dataset I** – used for testing the trained agent and verifying its performance, and it also contains the cases that can be solved by the PF solver; **testing dataset II** – used for testing the trained DRL agent on some “dangerous” situations, which initially diverge during the PF calculation due to the unreasonable generator settings.

By following the aforementioned data generating procedures, the dataset information for the testing systems in this paper is shown in TABLE I.

The performance evaluation of the trained DNN is based on (1) whether the solution is feasible and (2) how close the solution is compared with mathematical solver instead of showing the loss values. To validate the performance of the trained agent, cost comparison in percentage (κ), success rate

and total running time are chosen as evaluation indices. Comparison in percentage (κ) is calculated as in Eq. (12) [12], where $cost_{agent}$ and $cost_{pips}$ represent the system cost obtained through the PPO agent and PIPS solver, respectively. The success rate represents the percentage among the testing data that the agent successfully solves the OPF problem without violating any constraints. The running time comparison is made by using a laptop with Intel i7-7700HQ CPU at 2.8GHz and 12GB RAM.

$$comparison\ in\ percentage\ (\kappa) = \frac{cost_{pips} - cost_{agent}}{cost_{pips}} \quad (12)$$

TABLE I
THE DATASET INFORMATION FOR THE TESTING SYSTEMS

Testing system	Num. of training dataset	Num. of testing dataset I	Num. of testing dataset II
IEEE 14-bus system	55000	17364	2000
Illinois 200-bus system	60000	20000	5000

A. The IEEE 14-bus system

The dimensions of the state and action space are 38 and 10 respectively in the IEEE 14-bus system. Originally there are no line flow limits in the original system model, and thus, a limit of 32 MVA on line 4-5 is used to test the agent performance. Under such circumstances, AC OPF solver based on semidefinite programming (runsdopf) from Matpower [5]) fails to recover the rank-1 matrix under the original loading condition, which means the OPF solution is more difficult to obtain. The z value in Eq. (7) is set as 120 in this case. The maximum episode length T is set as 5.

Three hidden layers with (380, 195, 100) neurons are applied in the actor NN and three hidden layers with (380, 44, 5) are applied in the critic NN in PPO. The training process for IL is shown in Fig. 7, where 99% of the data in the training dataset is used as a sub-training dataset and the remaining 1% data is regarded as a sub-testing dataset for the IL process.

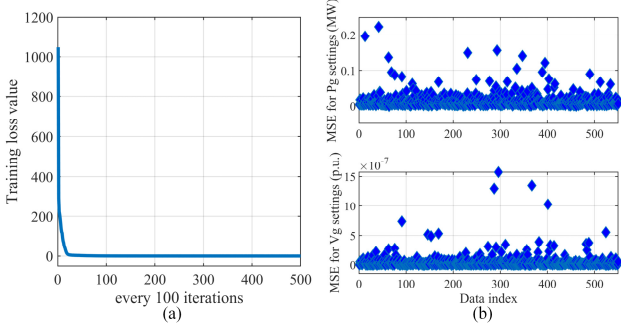


Fig. 7. IL results. (a) Training loss curve. (b) Loss during the testing process.

The losses from Eq. (10) are very small, as indicated in Fig. 7, which validates the structure of actor NN. Then we apply this actor NN initialized by IL to perform the OPF task in testing dataset I, and the results are shown in TABLE II.

From TABLE II, it is observed that though the training and testing losses in IL become very small, there are still 10,226 out of 17,364 cases in the testing dataset I that violate the system constraints and most of the violations are on the modified line flow, due to the smaller feasible regions of the modified system. This indicates that the applying DL training technique alone is

not enough in those difficult cases with the relatively small feasible region.

To further prove the effectiveness of PPO, the initialized policy is generated where only 9,900 out of 55,000 training cases are employed to perform IL. Afterward, the agent with this initialization is trained for 2 epochs with PPO, where KL_tar is set to 0.03. Moreover, to verify the significance of the IL for the agent's training performance, the PPO training without IL is also performed. Fig. 8 illustrates the PPO training processes, where the entropy is applied to evaluate how deterministic the policy becomes during training (how certain the PPO agent becomes). It can be observed from Fig. 8 that the decreasing policy entropies and the increasing rescaled mean rewards verify that both agents are effectively learning control policies during the training process.

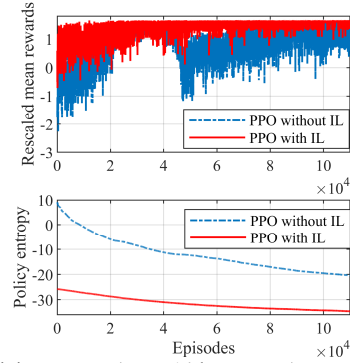


Fig. 8. PPO training process (IEEE 14-bus system).

Then, two PPO agents are trained without and with IL to perform the OPF task on the testing dataset I, and their results are shown in TABLE II and Fig. 9. From TABLE II, there are still 1,420 out of 17,364 testing cases that either violate the constraints or diverge after 2-epoch of training without IL, which suggests that it would take longer training time for the agent to converge under such circumstance. In contrast, the PPO agent with IL performs much better in all cases using the same setting. More importantly, the total generation costs obtained from the agent are very close to those calculated directly from PIPS, where the average and maximum absolute value of κ shown in Eq. (12) are only 0.597% and 1.75% higher, respectively. This comparison clearly demonstrates the significance and superior performance when using IL for training PPO agents. In addition, the trained agent is capable of controlling the system to achieve the optimal cost within just one step in 99.76% of the 17,364 testing cases. Furthermore, to obtain (sub)optimal solutions for the 17,364 testing cases, the running time from the PIPS solver costs 6.184 hours, while it only takes 0.863 hours from the proposed method, indicating a ~ 7 times of speedup.

TABLE II
COMPARISON OF PPO AGENTS' PERFORMANCE ON TESTING DATASET I FOR THE MODIFIED IEEE 14-BUS SYSTEM

Training method	number of success data	number of failed data	success rate	max $ \kappa $ among success data	min $ \kappa $ among success data	average $ \kappa $ among success data
IL	7138	10226	41.11%	0.33%	1.93e-5%	1.29e-2%
PPO	15944	1420	91.82%	17.55%	0.56%	3.27%
PPO with IL	17364	0	100%	1.75%	0.21%	0.597%

Moreover, Fig. 10 illustrates the performance of the agent with IL in the testing dataset II, which contains the data that the Newton-Raphson PF solver initially diverges. One can observe that the trained agent can still solve the OPF problem well under the “dangerous” conditions, and all the cases can be solved within a maximum of 2 steps. From TABLE II, Fig. 9, and Fig. 10, the effectiveness of the proposed method is verified in the IEEE 14-bus system.

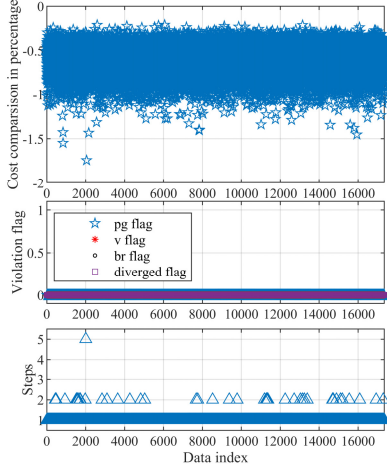


Fig. 9. PPO performance with IL for solving the OPF task on testing dataset I (IEEE 14-bus system).

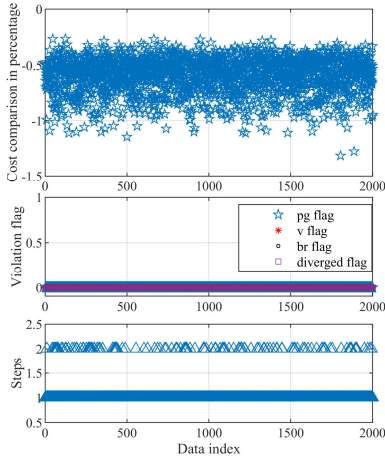


Fig. 10. PPO performance with IL for solving the OPF task on testing dataset II (IEEE 14-bus system).

B. The Illinois 200-bus system

The Illinois 200-bus system is also adopted to demonstrate the performance of the proposed approach in a larger and more complex system. The dimensions of the state and action space are 476 and 76, respectively. The thermal limit of line 124-123 is reduced from 400MW into 230MW to make the AC OPF problem more difficult to solve. All other thermal limits of lines are not modified. The z value in Eq. (7) is set as 500 in this case. The maximum episode length T is set as 5.

Since the action space is much larger, a deeper NN containing eight hidden layers with (2,048, 1,024, 1,024, 1,024, 512, 512, 512) neurons is applied as the actor NN. And the NN consisting of three hidden layers with (4,760, 154, 5) is utilized as the critic NN. Besides, IL is applied to the training dataset as initial weights for training PPO agents.

TABLE III illustrates the performance of the NN with just IL on the testing dataset I. The results show 8,702 out of 20,000 cases still have violations of the system constraints. The PPO agents with and without IL are both trained for 4 epochs, where KL_tar is set as 0.01. The corresponding PPO training process for the 200-bus system is shown in Fig. 11, which reflects that the learning process with initialization through IL is much more effective than that of the case without IL. The agent without IL does not achieve the same level of reward as the agent with IL does. Fig. 8 and Figs. 11 imply that the benefits of initialization with IL would be much more obvious in larger systems.

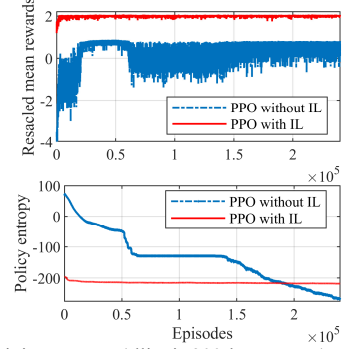


Fig. 11. PPO training process (Illinois 200-bus system).

Fig. 12 and TABLE III illustrate the performance of the trained agent with IL on testing dataset I, which shows that the agent is capable of controlling the system to achieve the optimal cost within 5 steps in 99.95% of 20,000 cases, in which 99.96% can be solved within just one step. The total generation cost resulting from the actions given by the agent is very close to those obtained from the PIPS, with the average and maximum absolute value of κ shown in Eq. (12) only around 0.61% and 1.65% higher, respectively. Moreover, to solve the 20,000 testing data, the running time of the PIPS is around 15 hours, whereas it only takes 2 hours for the proposed method, which is around 7.5 times faster than the conventional solver.

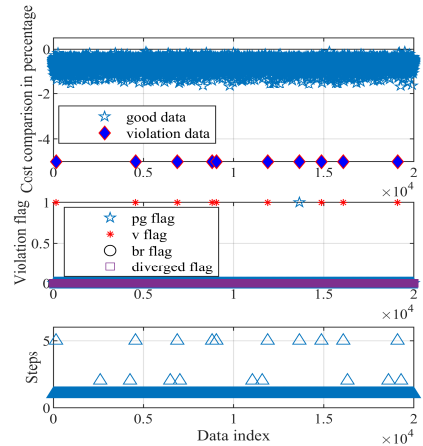


Fig. 12. Performance of PPO agent with IL on the testing dataset I (Illinois 200-bus system).

Additionally, the performance of the agent with IL is also tested on the testing dataset II with “dangerous” conditions, and the results are shown in Fig. 13. It can be observed that the trained agent can solve 99.94% of the 5000 cases with “dangerous” conditions, which attributes to the special design

in the actor NN introduced in Section III.

TABLE III
COMPARISON OF PPO AGENTS' PERFORMANCE ON TESTING DATASET I FOR
THE MODIFIED ILLINOIS 200-BUS SYSTEM

Training method	number of success data	number of failed data	success rate	max $ k $ among success data	min $ k $ among success data	average $ k $ among success data
IL	11298	8702	56.49%	1.28%	8.6e-4%	0.12%
PPO with IL	19990	10	99.95%	1.65%	0.11%	0.61%

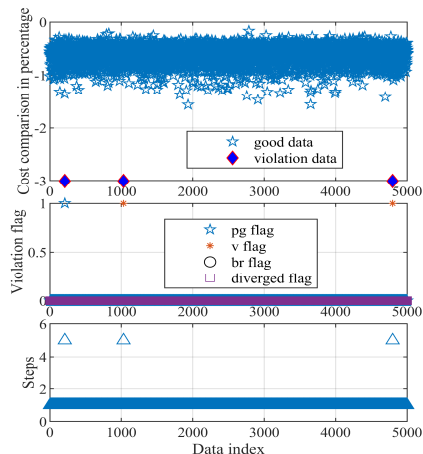


Fig. 13. OPF task results of testing dataset II (Illinois 200-bus system).

V. CONCLUSION

In this paper, a new method of deriving fast AC OPF solution by applying the state-of-the-art DRL algorithm, PPO, is presented, which adopts the IL technique as initial NN weights for expediting the training process. The IEEE 14-bus system and a realistic Illinois-200 bus system are utilized to verify the proposed approach. The optimal costs from the proposed method are very close to those directly calculated from the PYPOWER AC OPF solver; however, the solution time improves by at least 7 times as compared to the conventional solver, which validates the effectiveness of the proposed method and manifests a great promise of adopting DRL techniques in the power system operations and control.

The future work includes studying on how to further improve the performance of the agent in terms of improving the optimality, increasing success rate, including N-1 and/or N-2 security constraints and reducing the number of steps, etc.

VI. REFERENCES

- [1] Y. Tang, K. Dvijotham, and S. Low, "Real time optimal power flow," *IEEE Trans. Smart Grid*, vol. 8, no. 6, pp. 2963–2973, Nov. 2017.
- [2] R. A. Jabr, "A primal-dual interior-point method to solve the optimal power flow dispatching problem," *Optimization and Eng.*, vol. 4, no. 4, pp. 309–336, Dec. 2003.
- [3] R.A. Jabr, "Radial distribution load flow using conic programming," *IEEE Trans. Power Syst.*, vol. 21, no. 3, pp. 1458–1459, Aug. 2006.
- [4] J. Lavaei, and S. H. Low, "Zero duality gap in optimal power flow," *IEEE Trans. Power System*, vol. 27, no. 1, pp. 92–107, Feb. 2012.
- [5] D. K. Molzahn, J. T. Holzer, B. C. Lesieutre, et al., "Implementation of a large-scale optimal power flow solver based on semidefinite programming," *IEEE Trans. Power Systems*, vol. 28, no. 4, pp. 3987–3998, Nov. 2013.
- [6] R. Madani, S. Sojoudi, and J. Lavaei, "Convex relaxation for optimal power flow problem: mesh networks," *IEEE Trans. Power Systems*, vol. 30, no. 1, pp. 199–211, Jan. 2015.
- [7] R. Madani, M. Ashraphijuo, and J. Lavaei, "Promises of conic relaxation for contingency-constrained optimal power flow problem," *IEEE Trans. Power System*, vol. 31, no. 2, pp. 199–211, Jan. 2015.
- [8] E. Dall'Anese and A. Simonetto, "Optimal Power Flow Pursuit," *IEEE Trans. on Smart Grid*, vol. 9, issue 2, pp.942–959, March 2018.
- [9] B. Donon, B. Donnot, I. Guyon, and A. Marot. "Graph neural solver for power systems." In 2019 International Joint Conference on Neural Networks (IJCNN), pp. 1–8. IEEE, 2019.
- [10] X. Pan, T. Zhao, and M. Chen, "DeepOPF: deep neural network for DC optimal power flow". In: arXiv preprint arXiv: 1905.04479 (2019).
- [11] D. Deka, and S. Misra, "Learning for DC-OPF: classifying active sets using neural nets". In: arXiv preprint arXiv: 1902.05607 (2019).
- [12] A. S. Zamzam, K. Baker, "Learning optimal solutions for extremely fast AC optimal power flow". In: arXiv preprint arXiv: 1910.01213 (2019).
- [13] F. Fioretto, T. W.K. MaK, and P. V. Hententryck, "Predicting AC optimal power flows: combining deep learning and lagrangian dual method". In: arXiv preprint arXiv: 1909.10461 (2019).
- [14] V. Francois-Lavet, P. Henderson, R. Islam, et al., "An introduction to deep reinforcement learning". In: arXiv preprint arXiv: 1811.12560 (2018).
- [15] Y. Xu, W. Zhang, W. Liu, et al., "Multiagent-based reinforcement learning for optimal reactive power dispatch," *IEEE Trans. Systems, man, and cybernetics, part C (Applications and Reviews)*, vol. 42, no. 6, pp. 1742–1751, Nov. 2012.
- [16] T. Yu, J. Liu, K. W. Chan, et al., "Distributed multi-step Q(λ) learning for optimal power flow of large-scale power grids," *Electrical Power and Energy Systems*, vol. 42, no. 1, pp. 614–620, Nov. 2012.
- [17] E. Mocanu, D. C. Mocanu, P. H. Nguyen, et al., "On-line building energy optimization using deep reinforcement learning," *IEEE Trans. Smart Grid*, vol. 10, no. 4, pp. 3698–3708, Jul. 2019.
- [18] R. Diao, Z. Wang, D. Shi, et al. "Autonomous voltage control for grid operation using deep reinforcement learning," In: arXiv preprint arXiv: 1904.10597 (2019).
- [19] J. Duan, D. Shi, R. Diao, et al. "Deep-reinforcement-learning-based autonomous voltage control for power grid operations," *IEEE Trans. Power Systems*, Sep. 2019.
- [20] Z. Yan, and Y. Xu, "Data-driven load frequency control for stochastic power systems: a deep reinforcement learning method with continuous action search," *IEEE Trans. Power Systems*, vol. 34, no. 2, pp. 1653–1656, Mar. 2019.
- [21] J. Schulman, F. Wolski, P. Dhariwal, et al., "Proximal policy optimization algorithms". In: arXiv preprint arXiv: 1707.06347 (2017).
- [22] Pypower 5.1.4, [Online]. Available: <https://pypi.org/project/PYPOWER/>
- [23] R. D. Zimmerman, C. E. Sanchez, and R. J. Thomas, "MATPOWER: steady-state operations, planning, and analysis tools for power systems research and education," *IEEE Trans. Power Systems*, vol. 26, no. 1, pp. 12–19, 2011.
- [24] R. S. Sutton, and A. G. Barto, *Reinforcement Learning – An Introduction*, 2nd ed., Cambridge, MA: MIT Press, 2018.
- [25] Y. LeCun, Y. Bengio, and G. Hinton. "Deep learning." *Nature* 521. (2015): 436–444.
- [26] H. Daumé III (2012). *A course in machine learning*. [Online]. Available: http://ciml.info/dl/v0_99/ciml-v0_99-all.pdf
- [27] V. Kurin. (2017, Aug). *Introduction to Imitation Learning*. [Online] Available: <https://blog.statsbot.co/introduction-to-imitation-learning-32334c3b1e7a>
- [28] J. Schulman, P. Moritz, S. Levine, et al. "High-dimensional continuous control using generalized advantage estimation". In: arXiv preprint arXiv: 1506.02438 (2015).
- [29] J. Schulman, S. Levine, P. Moritz, et al. "Trust region policy optimization". In: arXiv preprint arXiv: 1502.05477 (2015).
- [30] G. Brockman, V. Cheung, L. Pettersson, et al. "OpenAI gym". In: arXiv preprint arXiv: 1606.01540 (2016).
- [31] F. Pedregosa, G. Varoquaux, J. Vanderplas. "Scikit-learn: Machine learning in Python," *Journal of machine learning research*, pp. 2825–2830, Oct. 2011.
- [32] D. J. C. MacKay, *Information theory, inference and learning algorithms*, Cambridge, U.K.: Cambridge University Press, 2003.
- [33] D. P. Kingma, J. Ba. "Adam: a method for stochastic optimization," In: arXiv preprint arXiv: 1412.6980 (2014).
- [34] Illinois Center for a Smarter Electric Grid (ICSEG), IEEE 14-Bus System. [Online]. Available: <https://icseg.iti.illinois.edu/ieee-14-bus-system/>
- [35] Electric Grid Test Case Repository, Illinois 200-Bus System: ACTIVSg200. [Online]. Available: <http://electricgrids.engr.tamu.edu/electric-grid-test-cases/activsg200/>